Delft University of Technology

Investigations of the Virtual Impedance Control Mode of Synchronverter in the Power Swing

Gonzalez-Longatt, Francisco M.; Rueda, José Luis; Palensky, Peter; Chamorro, Harold R.

Important note
To cite this publication, please use the final published version (if applicable).
Please check the document version above.

Investigations of the Virtual Impedance Control Mode of Synchronverter in the Power Swing

Francisco M. Gonzalez-Longatt
Department of Electrical Engineering, Information Technology and Cybernetics
University of South Eastern Norway
Porsgrunn, Norway
fglongatt@fglongatt.org

Jose Luis Rueda, Peter Palensky
Department of Electrical Sustainable Energy
Delft University of Technology
Delft, The Netherlands
J.L.RuedaTorres@tudelft.nl
P.Palensky@tudelft.nl

Harold Chamorro
School of Electrical Engineering and Computer Science
KTH, Royal Institute of Technology
Stockholm, Sweden
hr.chamo@ieee.org

Abstract—**Power electronic converter (PEC) is a key element for the successful integration of novel technologies, PEC working as inverter at novel generation technologies are the decisive components to zero-net carbon emissions in the electricity systems. The colossal penetration of IBG tends to produce several issues in the power networks. There is a tendency to agree that the voltage source converters (VSCs) empowered with the so-called grid forming (GFR) control may provide a long-term solution for the inverter-based generation-dominated power systems. This scientific paper presents an investigation (based on numerical simulations) of the effect of the virtual impedance control mode of one grid forming control technique in the power swing of power systems. Numerical time-domain simulations on test systems are used to assess the effect of the virtual impedance (VI) control mode of the synchronverter (SynC) during a power swing. In both cases, the simulation-based investigation has shown evidence of using high and low virtual impedance in both cases, considering constant impedance and proportional over-current limitation. However, this paper concludes that further assessments are required.**

Keywords—converters, control, power swing, stability, virtual impedance.

I. Introduction

The growing integration of renewable generation is crucial for reaching the ambitious goal of zero-net. A totally decarbonised energy system requires maximising the use of renewable generation, which means a colossal penetration level of solar photovoltaic and wind power. However, that environmentally friendly and weather-dependent generation typically requires the use of a power electronic converter as an interface to the power network, and it imposes many challenges from the operation, planning and economics of the power system [1], [2], [3].

Solar photovoltaic (PV) and wind power (WP) are renewable-based generation resources typically known as inverter-based generation (IBR). It is because the power electronic converter (PEC) operating in inverter mode provides the interface to the power grid at the time that defines the interaction between the generator at the power systems. The IBG is a critical element in realising the energy transition toward a zero net grid [4], [5].

Many electricity system operators (ESOs) around the world are concerned regarding the latent impact of the massive penetration of the inverter-based generation (IBR) [1], [6]. However, it must be clear that the massive integration of renewable that motivates the enormous penetration of IBG is one side of the main challenges. On the other hand,

decommissioning large coal and nuclear power plants reduces the number of synchronous machines (SM) connected to the power systems [7]. Those two situations are causing two groups of issues: (i) the problems originated from the integration of the IBG itself and (ii) the problem caused by the substitution of SG-based power plants by the environmentally friendly IBG power plants.

Many scientific publications and research projects have been working on assessing the consequence of the low rotational inertia in modern power systems, and some other publications and projects. Those initiatives have identified two fundamental concerns [8], [9]: (i) The new generation mix and novel technologies are causing a reduction in sources rotational inertia with the systemic impact and (ii) very limited short circuit fault levelsFIBR when compared with the traditional SG-dominated power systems.

When proposing solutions to the issues related to the IBG-dominated power system two possible options are considered based on the time horizon of the proposed solutions: short-term and long-term. A comprehensive discussion of all of them is beyond the scope of this research paper, but it is consensus that one potential long-term solution is implementing very specific control techniques at the grid side inverter (GSI) based on VSC, the most promising techniques reported in recent times is the GFR control.

The research team involved in this research paper has already published a glimpse at the dynamic performance of the IBR enabled with GFR control technique during fault conditions [11].

This research paper presents an investigation (based on numerical simulations) of the effect of the virtual impedance control mode of one grid forming control technique in the power swing of power systems. In this scientific, one grid forming technique is considered, the so-called synchronverter (SynC). A simple but representative test system is used for the experimental investigations of the power swings; it consists of an IBR enabled with grid forming converter technique -SynC -this IBG is connected to an infinite busbar. The authors have assessed the short circuit currents in different scenarios in [11] and in this paper, the main concern is the systemic point of view related to power swings. Section II shows details the GFR control technique applied to IBR, specifically the well-known SynC. Section III is dedicated to presenting the numerical results of the experiments to investigate the effect of the virtual impedance control on the power swings during and after a fault condition. Finally, section V shows the most important findings and conclusions of this research paper.

II. SYNCHRONVERTER CONTROLLER

A VSC enabled with GFR control technique allows the IBG to work as an ideal controllable voltage source behind a controllable (virtual) impedance. The circuit-based approach allows the PEC to mimic the most simple behaviour of a classic SG (the mimic is only within the possibilities of the PEC).

In this research paper, the GFR control implemented is the well-known SynC. In this case, the IBR is modelled by using an ideal VSC modelled as a controllable AC voltage source (v) behind low-output impedance (Z_{vi}); details of the circuit model are shown in Fig. 1.
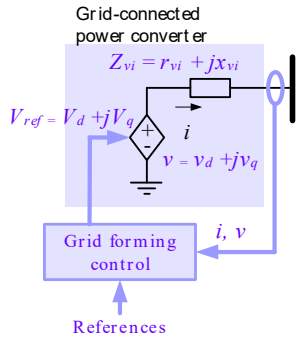

Fig. 1. Circuit diagram showing a GFM converter considering the concept of virtual impedance (VI) -Z_{vi}.

The control of the PEC is based on a stationary rotating dq-frame, an VI (Z_{vi}) is connected in series to a controllable voltage source, the real and imaginary components of the VI are defined as: $Z_{vi} = r_{vi} + jx_{vi}$, where r_{vi} is the virtual resistance and x_{vi} represents the virtual reactance. The voltage drop across the VI is represented using the d-axis and q-axis as (Δ means drops) [11]:

$$\begin{aligned} \Delta v_{vi,d} = r_{vi}i_d - x_{vi}i_q \\ \Delta v_{vi,q} = r_{vi}i_q + x_{vi}i_d \end{aligned} \tag{1}$$

The first scientific publication reporting the idea of the SynC was "*Synchronverters: Inverters that mimic synchronous generators*" proposed by Q. Zhong and G. Weiss, 2011 [14]. In this paper, the authors used the SynC model presented in [14]. It is essential to differentiate the SynC concept and the well-known virtual synchronous machine (VSM); the distinction is in implementing the electromechanics dynamic using versions of the swing equation. The SynC control technique considers the mechanical dynamics of the hypothetical synchronous machine expressed in terms of torques balance [11]:

$$\begin{cases} T_{acel}\dfrac{d\theta^2(t)}{dt^2} = T_{ref} - T_{actual} - D_p \dfrac{d\theta(t)}{dt} \\ \dfrac{d\theta(t)}{dt} = (\omega_r - \omega_{ref}) \end{cases} \tag{2}$$

where the T_{actual} is sed to represent the electrical toque, and it is calculated as:

$$T_{actual} = M_f i_f \sin\theta \tag{3}$$

In the previous equation, i_f is used to represent the current circulating through an imaginary field (rotor) winding of the SynC. The hypothetical field winding is supplied by an adjustable DC current source. M_f is used to mimic a

hypothetical mutual inductance between the imaginary field winding and the three stator windings. On the other hand, the internal induced voltage (v) of the circuit model is characterised as:

$$v = \frac{d\theta}{dt} M_f i_f \sin\theta \tag{4}$$

Considering the previously described model, the active (p_{calc}) and the reactive (q_{calc}) power flows can be obtained as:

$$\begin{cases} p_{calc} = \dfrac{d\theta}{dt} M_f i_f i \sin\theta \\ q_{calc} = -\dfrac{d\theta}{dt} M_f i_f i \cos\theta \end{cases} \tag{5}$$

A very well-known and used control mechanism of the reactive power flow is the use of the called Q-V droop. The droop control calculates the reactive power setpoint based on the voltage deviation measured from a reference point. The reactive power flow error (Δq) is obtained by using the following equation:

$$\Delta q = q_{ref} - q_{calc} - D_q\left(v - v_{ref}\right) \tag{6}$$

where q_{ref} represents reactive power reference, q_{calc} indicates the calculated reactive power flow, v is the measured voltage at the terminals of the SynC, v_{ref} is the reference voltage (1.0 pu when the rated power is considered), and the relationship between voltage and reactive power is defined by a proportionally constant D_q known as the voltage droop coefficient.

A. Current Limiting control of virtual impedance

The SMs have a natural capacity for tolerating overloads, especially during short circuit conditions. However, the commuting semiconductors used in the modern PECs are very sensible and fragile against overcurrent. A current control loop could be added to the GFM control to avoid a potentially dangerous (for the semiconductors) overcurrent condition during a short circuit. However, the GFM property is lost when it is most needed!

The VI controller may be used to adapt the VI parameters ($Z_{vi} = r_{vi} + jx_{vi}$) to the grid condition. One possible control objective of this control loop is to increase the VI (Z_{vi}) during a short circuit and avoid damage to the semiconductor in the PEC. The VI is adjusted in proportion to the low pass filtered current absolute value $|i|$ (see Fig.1) when a certain threshold i_{lim} is exceeded.

$$z_{vi} = \begin{cases} r_{vi} + jx_{vi}, & \text{if } |i| \leq i_{\lim} \\ \left(k_{pr}r_{vi} + jk_{px}x_{vi}\right)\left(|i| - i_{\lim}\right) + r_{vi} + jx_{vi} & \text{if } |i| > i_{\lim} \end{cases} \tag{7}$$

where k_{pr} and k_{px} are the proportional factors for the virtual resistor and virtual reactance, respectively.

In this scientific paper, the main interest is to assess the impact of the parameters used in the virtual impedance on the power swing; as a consequence, the values of r_{vi} and x_{vi} are considered parameters to explore.

III. EXPERIMENTS

This paper uses a simple test system to investigate the impact of VI control on the power swings. The test systems consist of a single machine connected to an infinite busbar,

also known as SMIB (single machine infinite bus). The power swing is excited in the test system by using a bolted three-phase sort circuit after it; the faulted transmission line is removed from the system (see Fig. 2).

For experimental purposes, the test system consists of a single IBR enabled with a SynC (data provided in Table I and II) it is connected to a very large equivalent power system (assumed as an infinite busbar), a step-up transformer (T_1) and two transmission lines (L_1 and L_2), and a step-down transformer (T_2) (see Fig. 2). Two loads are added, one at the bus ② and the other at ③ and both are modelled as constant power. The experiments presented in this section are dedicated to evaluating the performance previous to the contingency during and after a bolted three-phase short circuit. The short circuit is located in the middle of the transmission line L1, and the L2 remains unaffected transmitting power to the infinite bus. The IBR is assumed to be a 210 MVA, 15.47 kV, pf = 0.8.
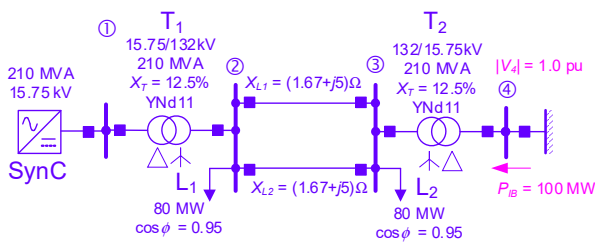

Fig. 2.   *Test System*: A single generation technology connected to an infinite bus.

A specific purpose co-simulation environment was developed for the experimental investigations in this scientific paper. The co-simulation framework is based on DIgSILENT PowerFactory, Python API and a Python script. DIgSILENT PowerFactory is used as a power system solution engine, and the interface and script in Python are used to automate the simulation and data management. Finally, MATLAB is used for post-processing the data and plotting the results.

A. Assessing the critical clearing time of SynC

The dynamic performance of the SynC during and after a short circuit is very different when compared to the SG_1. The first clear difference between the synchronous machine and the power electronic converter is the transient overload capacity. The current limitation of a power electronic converter equipped with a SynC controller is clearly evident in Fig. 3. The virtual impedance controller is designed to calculate the real and reactive voltage drop across the virtual impedance (see details at equation (1)), including a current limiter. However, the current limitation is fully enforced during the final output voltage calculation; the current implementation used in this paper considers a current magnitude limitation of 1.2 pu. Fig. 3 shows how the current magnitude reaches 9.23 kA during the fault condition (stable and unstable conditions) but then following the clearing of the fault; the current is still at the limit during the voltage recovery period. The limited overcurrent period following the fault clearing is caused by the amount of reactive power required to recover the voltage during the post-contingency condition. Therefore, the SynC controller tries to mimic the dynamic performance of the synchronous machine; to do so, it follows a second-order linear differential equation to imitate the rotor angle and frequency of a fictitious synchronous generator, which is presented in (2). The model includes an acceleration time (T_{acel}) of the identical value of the SG_1 for comparative

purposes. In this paper, the authors consider the fictitious rotor angle created by the SynC controller as the primary indicator to describe two possible operation conditions, the so-called stable transient rotor angle where the response no produces a phase jump. Using time-domain simulation, the authors identified that the maximum time that the fault can be cleared without producing a phase jump to a negative angle was t_{clear} = 4.0 secs; this situation is depicted in Fig. 3.
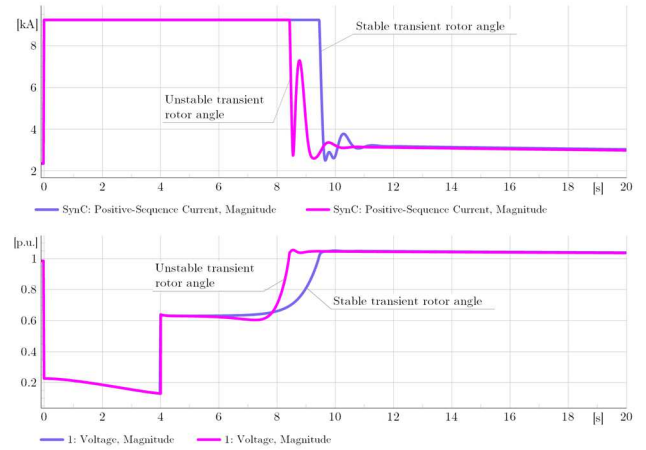

Fig. 3.   Plot of current ($|I|$) and voltage ($|V|$) magnitude of SynC during a transient rotor angle stability. Stable condition when fault is cleared at t = 4.0 sec and unstable at t = 4.01 sec.
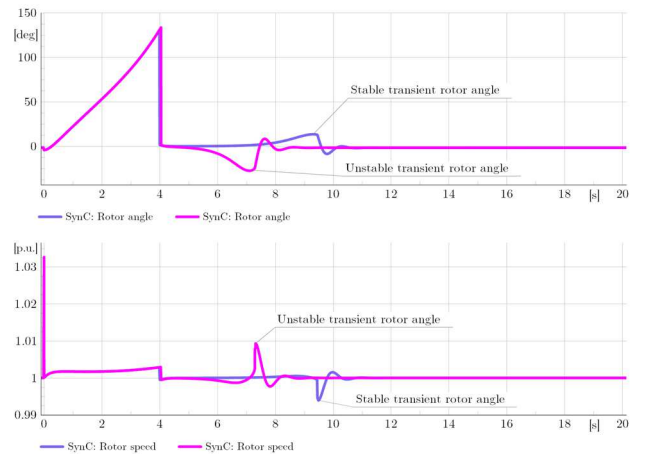

Fig. 4.   Plot of rotor angle (θ_r) and speed (ω_r) of SynC during a transient rotor angle stability. Stable condition when fault is cleared at t = 4.0 sec and unstable at t = 4.01 sec.

Fig. 4 made clear the concept used in this paper for stable and unstable transient rotor angle; the stable trajectory of the active and reactive power involves both spending the majority of the trajectory inside the positive region of active power. However, an unstable condition made the trajectory spend most of the time in the negative P-semi-plane (P<0). A fascinating aspect of the PQ-trajectory is that in plotting the stable and unstable conditions, the semicircle defining the locus of constant apparent power ($|S|$= constant) is depicted. Fig. 5 shows the shows locus of the impedance magnitude ($|Z|$ in primary Ohms) measured at the terminal connected to ② of the faulted transmission line (L_1) when compared to the one produced by the synchronous generator for similar conditions (stable and unstable), it results in evident dissimilarities between them. An unstable condition sends the RX trajectory to the negative reactance semi-plane (X<0), but the SynC controller provides a less distinctive trajectory.
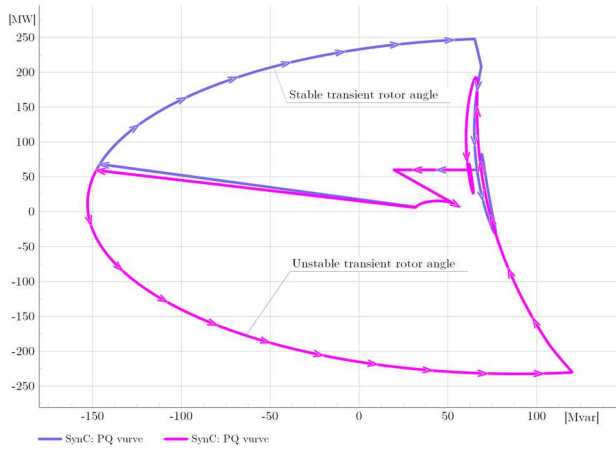
Fig. 5. Plot of active power versus reactive power (*PQ*-plane) of SynC during a transient rotor angle stability. Stable condition when fault is cleared at $t = 4.0$ sec and unstable at $t = 4.01$ sec.
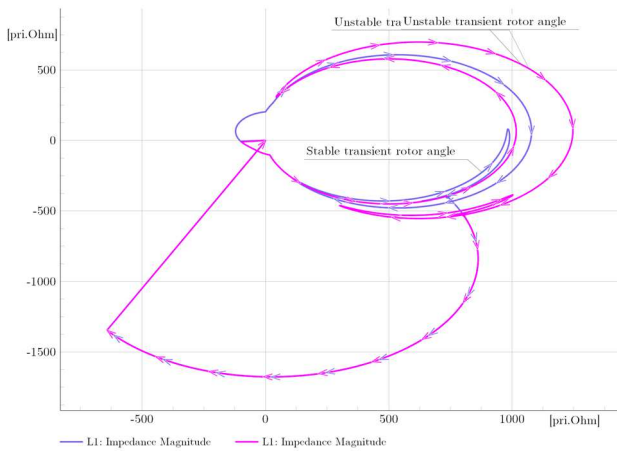

Fig. 6. Plot of active power versus reactive power (*RX*-plane) of SynC during a transient rotor angle stability. Stable condition when fault is cleared at $t = 4.0$ sec and unstable at $t = 4.01$ sec.

B. Assessing the Effect of the VI

The effect of the virtual impedance controller is assessed in this paper by considering a set of scenarios shown in Table III. The real and imaginary parts of the virtual impedance are referred to as r_{vi}, the resistance and x_{vi} the reactance of the virtual impedance, two sets of values are used (low: 0.06 pu and high: 0.012 pu). This scientific paper considers two possible control modes for the virtual impedance, constant impedance and propositional overcurrent limitation.

Fig. 7 to 10 show the simulation results of the digital simulations. Each figure consists of four plots, the magnitude of the current and voltage magnitude at the terminal of the IBR, the active power versus reactive power (*PQ*-plane), and resistance versus reactance (*RX*-plane). Traditionally the power swing refers to the power flow variations in the power system caused by the electromechanical proposes during and after a large disturbance (e.g., a short circuit). The power swing is plotted in the *R-X*-plane as typically measured by the distance protections installed in the transmission system. Each case's clearing time is used to assess the performance of the so-called stable and unstable transient rotor angle swing. Using a low magnitude of the virtual impedance causes a deeper and slow post contingency voltage recuperation for shorter clearing times, more than 4 seconds for a clearing time of $t = 3.9$ sec. The use of high VI and propositional overcurrent

limitation tends to produce unstable power swing compared to low virtual impedance and constant impedance.
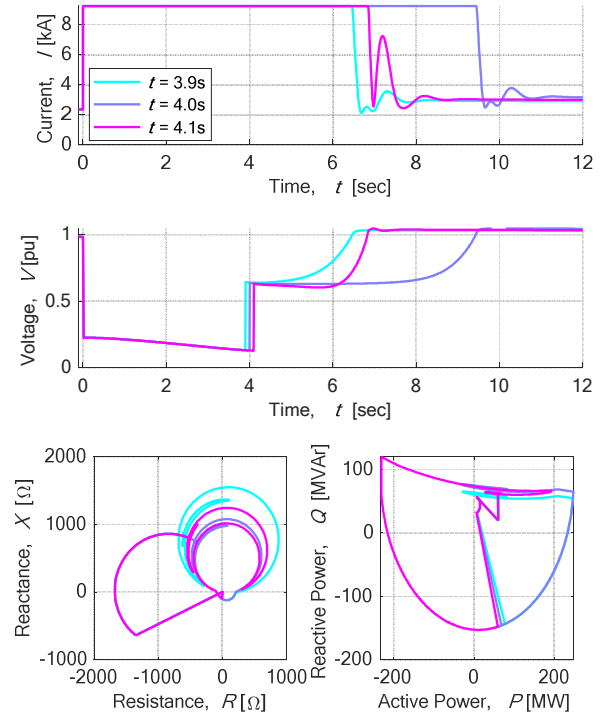

Fig. 7. *Case 0*: Time-domain plots of current (I), terminal voltage (V), active power versus reactive power (*PQ*-plane), resistance versus reactance (*RX*-plane).
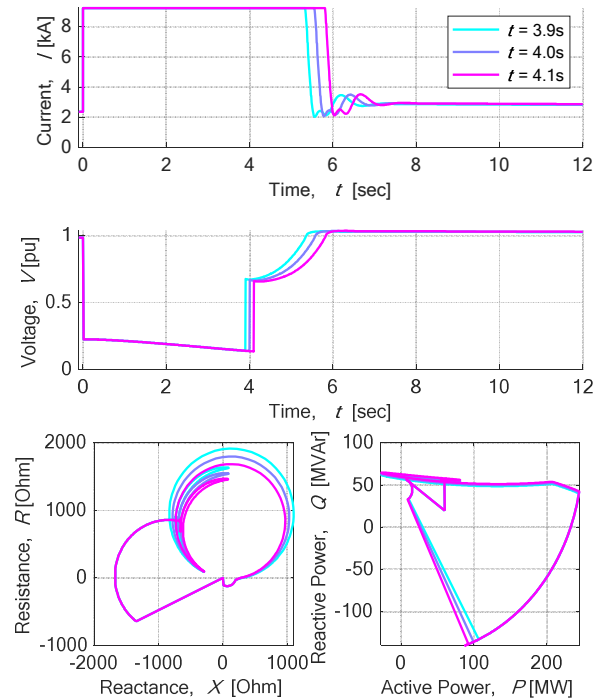

Fig. 8. *Case 1*: Time-domain plots of current (*I*), terminal voltage (*V*), active power versus reactive power (*PQ*-plane), and resistance versus reactance (*RX*-plane).

IV. CONCLUSIONS

The use of IBR with grid forming control technique is appraised as a potential solution to the massive deployment of power converter-based technologies and the reduction of the volume of synchronous generators connected to the power

systems. Many GFM control techniques are available; in this paper, the SynC technique is investigated, and the impact of the virtual impedance on the power swings. It has been identified that having low virtual impedance values allows better control of the voltage recovery and the post contingency current. From the power swing point of view, it has been found that high virtual impedance together with a constant impedance control model creates less harmful power flow oscillations. This preliminary assessment has made evident the need for a more detailed investigation of the power swing as the performance of the virtual impedance control has a strong effect on the performance not only during fault conditions but also post-contingency.
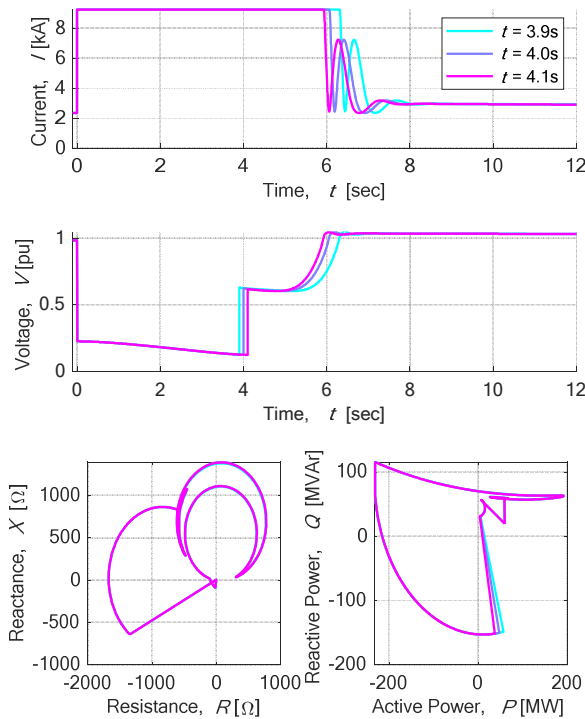
ACKNOWLEDGEMENT

Fig. 9. *Case 2*: Time-domain plots of current (I), terminal voltage (V), active power versus reactive power (*PQ*-plane), and resistance versus reactance (*RX*-plane).

TABLE I.   MAIN PARAMETERS OF THE SYNC CONTROL MODEL

Description	Variable	Value
Acceleration time	T_{acel}	18.36 sec
Damping coefficient	D_p	100.00pu
Voltage control gain	K_p	1000 pu
Reactive power drop coefficient	D_q	20.00 pu
Damping filter cut-off frequency	ω_r	0.00 rad/sec

TABLE II.   MAIN PARAMETERS OF THE VI USED IN THE SYNC CONTROL MODEL

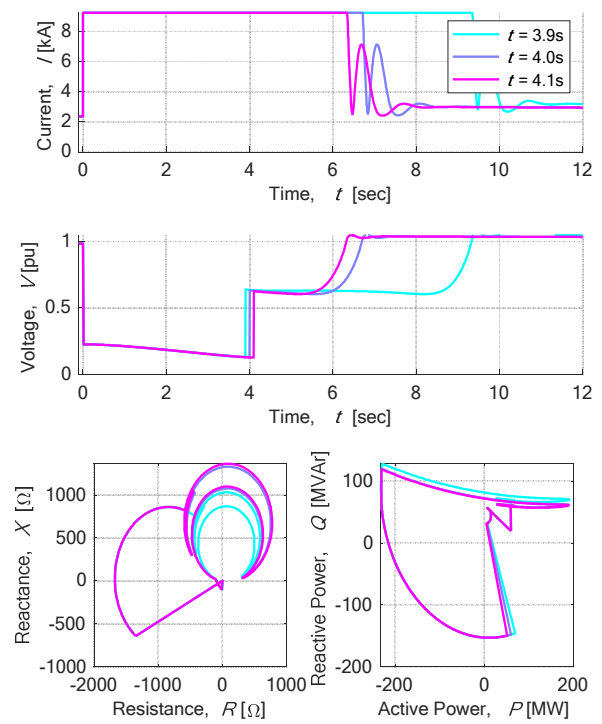| Description	Variable	Value
Limit of overcurrent	I_{lim}	1.01 pu
Proportional factor of additional resistance	k_{pr}	8.00 pu
Proportional factor of additional reactance	k_{px}	8.00 pu
Time constant of low pass filter	T_{lpf}	0.0001 sec

Fig. 10. *Case 3*: Time-domain plots of current (*I*), terminal voltage (*V*), active power versus reactive power (*PQ*-plane), and resistance versus reactance (*RX*-plane).

TABLE III.   SIMULATION CASES USED TO INVESTIGATE THE EFFECT OF THE VIRTUAL IMPEDANCE CONTROLLER.

Case	Virtual impedance		Control mode*
	Resistance [pu]	Reactance [pu]	
0	0.006	0.006	1
1	0.012	0.012	1
2	0.006	0.006	0
3	0.012	0.012	0

*: 0 = constant impedance, 1 = Proportional over-current limitation.

REFERENCES

[1] Y. Rajbhandari *et al.*, "Load prioritisation technique to guarantee the continuous electric supply for essential loads in rural microgrids," *Int. J. Electr. Power Energy Syst.*, vol. 134, no. November 2020, p. 107398, Jan. 2022, doi: 10.1016/j.ijepes.2021.107398.

[2] A. Shrestha, B. Ghimire, and F. Gonzalez-Longatt, "A Bayesian Model to Forecast the Time Series Kinetic Energy Data for a Power System," *Energies*, vol. 14, no. 11, p. 3299, Jun. 2021, doi: 10.3390/en14113299.

[3] A. Shrestha and F. Gonzalez-Longatt, "Frequency Stability Issues and Research Opportunities in Converter Dominated Power System," *Energies*, vol. 14, no. 14, p. 4184, Jul. 2021, doi: 10.3390/en14144184.

[4] F. Gonzalez-Longatt, M. N. Acosta, H. R. Chamorro, and Jose Luis Rueda, "Power Converters Dominated Power Systems," in *Modelling and Simulation of Power Electronic Converter controlled Power Systems in PowerFactory*, First Edit., F. Gonzalez-Longatt and Jose Luis Rueda, Eds. Switzerland: Springer Nature Switzerland AG, 2021.

[5] F. S. Gorostiza and F. Gonzalez-Longatt, "Deep Reinforcement Learning-Based Controller for SOC Management of Multi-Electrical Energy Storage System," *IEEE Trans. Smart Grid*, pp. 1–1, 2020, doi: 10.1109/TSG.2020.2996274.

[6] V. Astapov, S. Trashchenkov, F. Gonzalez-Longatt, and D. Topic, "Performance Assessment of TSO–DSO using Volt-Var Control at Smart-Inverters," *Int. J. Electr. Comput. Eng. Syst.*, vol. 13, no. 1, pp. 48–61, Feb. 2022, doi: 10.32985/ijeces.13.1.6.

[7] H. Chamorro, A. Guel-Cortez, E. Kim, F. Gonzalez-Longat, A. Ortega, and W. Martinez, "Information Length Quantification and Forecasting of Power Systems Kinetic Energy," *IEEE Trans. Power Syst.*, vol. 8950, no. c, pp. 1–1, 2022, doi: 10.1109/TPWRS.2022.3146314.

[8] "High Penetration of Power Electronic Interfaced Power Sources and the Potential Contribution of Grid Forming Converters European Network of Transmission System Operators for Electricity ENTSO-E Technical Group on High Penetration of Power Electronic Interfaced Power Sources." Accessed: Mar. 30, 2021. [Online]. Available: www.entsoe.eu.

[9] Australian Energy Market Operator, "Black System South Australia 28 September 2016," 2017. Accessed: Mar. 30, 2021. [Online]. Available: www.aemo.com.au.

[10] IEEFA, "Australia's Opportunity To Plan Ahead for a Secure Zero-Emissions Electricity Grid Towards Ending the Reliance on Inertia for Grid Stability," 2021.

[11] M. Habibullah, F. Gonzalez-Longatt, M. N. Acosta Montalvo, H. R. . Chamorro, J. L. Rueda, and P. Palensky, "On Short Circuit of Grid-Forming Converters Controllers: A glance of the Dynamic Behaviour,"

in *2021 IEEE PES Innovative Smart Grid Technologies Conference - Latin America (ISGT Latin America)*, Sep. 2021, pp. 1–5, doi: 10.1109/ISGTLatinAmerica52371.2021.9543017.

[12] National Grid, "System Operability Framework 2016," *UK Electr. Transm.*, no. November, pp. 68–72, 2016, Accessed: Mar. 30, 2021. [Online]. Available: www.nationalgrid.com/sof.

[13] N. Hatziargyriou *et al.*, "Stability definitions and characterisation of dynamic behavior in systems with high penetration of power electronic interfaced technologies," Dec. 2020. doi: 10.1109/JSYST.2015.2444893.

[14] Q. C. Zhong and G. Weiss, "Synchronverters: Inverters that mimic synchronous generators," *IEEE Trans. Ind. Electron.*, vol. 58, no. 4, pp. 1259–1267, Apr. 2011, doi: 10.1109/TIE.2010.2048839.